Impact of substituting K_2O for Na_2O on physico-chemical properties and in vitro bioactivity of bioactive glass S53P4

Sinitsyna, Polina; Engblom, Markus; Hupa, Leena

Published in:
Open Ceramics

DOI:
10.1016/j.oceram.2023.100440

Published: 01/12/2023

Document Version
Final published version

Document License
CC BY-NC-ND

Open Ceramics 16 (2023) 100440

Contents lists available at ScienceDirect

Open Ceramics

journal homepage: www.sciencedirect.com/journal/open-ceramics

Impact of substituting K_2O for Na_2O on physico-chemical properties and *in vitro* bioactivity of bioactive glass S53P4

Polina Sinitsyna *, Markus Engblom, Leena Hupa **

Laboratory of Molecular Science and Engineering, Åbo Akademi University, Henrikinkatu 2, 20500, Turku, Finland

ARTICLE INFO

Handling Editor: Dr P Colombo

Keywords:
Mixed-alkali effect
Ion release
Bioactive glass S53P4
Static dissolution
Dynamic dissolution

ABSTRACT

The impact of substituting K_2O for Na_2O (0–100%) on the physico-chemical and bioactive properties of bioactive glass S53P4 was studied. The thermal properties were evaluated using differential thermal analysis and high-temperature microscopy. Ion release kinetics was measured in static and dynamic TRIS-buffer and SBF using inductively coupled plasma optical emission spectroscopy. Substituting K_2O for Na_2O showed a mixed-alkali effect (MAE) for the thermal properties with a minimum value for the glass containing around 20% K_2O. The hot-working range increased with the potassium content. The glass with 66% of Na_2O replaced with K_2O exhibited MAE in static TRIS by giving the biggest pH change and ion release at 24 h. The same glass showed the lowest pH and Si species release in dynamic SBF at the longest dissolution time, 72 h. Both single-alkali glasses showed higher *in vitro* bioactivity in dynamic SBF. The results provide tools for tailoring new bioactive glass compositions with desired properties.

1. Introduction

The first bioactive glass, Bioglass® 45S5, discovered by Prof. Hench in 1969, has been in clinical use since 1985 [1]. Bioglass® 45S5, consisting of the four oxides Na_2O, CaO, P_2O_5, and SiO_2, gradually dissolves in body fluids while forming a hydroxycarbonate apatite (HCA) surface layer with a similar composition as the apatite mineral in bone [2]. However, due to its relatively low SiO_2 content (45 wt%, 46.1 mol.%), 45S5 has a high tendency to crystallise in thermal treatments, challenging the manufacture of hot-worked products [3]. Another commercial silicate-based bioactive glass, Bonalive® S53P4 (in mol.%: 53.9 SiO_2, 22.7 Na_2O, 21.8 CaO, 1.7 P_2O_5), also crystallises readily but allows limited hot-working [4]. Many attempts have been made to develop bioactive glass compositions which do not crystallise during sintering into porous tissue engineering scaffolds. Adding glass modifier oxides, such as K_2O, MgO, and B_2O_3, has extended the hot-working range [5–7]. Brink et al. investigated the influence of chemical composition on the thermal properties of 26 bioactive glasses in the Na_2O–K_2O–CaO–MgO–SiO_2–P_2O_5–B_2O_3 system [6]. The K_2O content in their study varied between 5 and 15 wt%. The glasses containing K_2O bonded with bone similarly to 45S5. One composition in the glass series by Brink et al., the bioactive glass 13–93 (in mol.%: 54.6 SiO_2, 6.0 Na_2O, 7.9 K_2O, 7.7 MgO, 22.1 CaO, 1.7 P_2O_5) showed desired hot-working and *in vivo* properties [5,6]. Glass 13–93 has been approved for *in vivo* use in EU [8,9]. It has higher network connectivity, contributing to lower bioactivity than 45S5 and S53P4, i.e., as less precipitated hydroxyapatite at the glass surface [10]. The presence of magnesium in the 13–93 composition reduces the bioactivity [3]. Glass 13–93 has later been used in the fabrication of tissue engineering scaffolds through the sintering of particles [11], the foam replication technique [12], freeze casting [13,14], and various additive techniques [15–17].

Bellucci et al. reported an increased sintering range when increasing the calcium content and replacing Na_2O with K_2O in bioactive glass 45S5 [18]. Recently, a silicate glass containing both Na_2O and K_2O (in mol.% 47.5 SiO_2, 10.0 Na_2O, 10.0 K_2O, 10.0 MgO, 10 CaO, 2.5 P_2O_5) was shown to have an intrinsic pro-osteogenic effect [19]. The *in vivo* studies using a fine-grained powder suggested an osteogenic effect and almost complete resorption in rabbit femurs after three months of implantation with simultaneous formation of laminar bone-like tissue. The observed osteointegration and the inflammatory response classified as non-severe of the new glass were taken as indications for its potential in bone healing applications. On the other hand, composites containing bioactive silicate glass fibres containing Na_2O and K_2O dissolved rapidly without any noticeable bone formation earlier reported for porous

* Corresponding author.
** Corresponding author.
E-mail addresses: polina.sinitsyna@abo.fi (P. Sinitsyna), leena.hupa@abo.fi (L. Hupa).

https://doi.org/10.1016/j.oceram.2023.100440
Received 22 March 2023; Received in revised form 8 August 2023; Accepted 20 August 2023
Available online 22 August 2023

implants of the same glass *in vivo* [20]. Substituting K_2O for Na_2O in silicate-based bioactive glasses suppresses the crystallisation tendency. However, the impact of the substitution on glass dissolution, especially tissue reactions, is not fully understood.

One common approach for adjusting the high-temperature properties of bioactive glasses is combining two (or more) alkali oxides to achieve the so-called mixed-alkali effect (MAE) [21]. Optimally, MAE provides deviation from the linear property changes with composition and leads to, e.g., improved chemical durability or lowered tendency to crystallisation for glasses containing two alkali oxides simultaneously. Partial replacing one alkali oxide with another, for example, Na^+ with K^+ or Li^+ with K^+, increases the hot-working temperature range of bioactive glasses owing to differences in ionic radii of the modifier ions [22,23]. The wider hot-working range, resulting from lower crystallisation tendency, has been explained by the reduced number of nucleation sites available for ion migration due to mixed alkalis in a glass. Therefore, a reduced ionic diffusivity is typical for MA glasses compared to single-alkali glass [24,25]. Besides the thermal properties, the MAE affects ion release and *in vitro* compatibility. When sodium (ion radius 102 p.m.) is replaced with potassium (138 p.m.), the network of silicate-based bioactive glasses expands, allowing faster ion release. Many studies have focused on MAE in bioactive glass 45S5 in which Na_2O is partially or wholly replaced by K_2O [21,26–30]. Cannillo et al. investigated the influence of the compositional effect on thermo-mechanical properties and bioactivity of potassium-based bioactive glass derived from the 45S5 composition [26]. The results of MAE in 45S5 indicated reduced crystallisation for the K-rich glass while maintaining the bioactivity [26,29]. Partly replacing one alkali oxide with another also helps to control ion release kinetics [28]. Ion release strongly depends on the glass composition, surface area/fluid volume ratio, fluid flow, particle size etc [31]. Static dissolution experiments in various dissolution media, including tris(hydroxymethyl)amino methane (TRIS) and simulated body fluid (SBF), are commonly used to measure the release of ions from the glasses [32–35]. Moreover, several studies have focused on the initial dynamic dissolution behaviour of MA glasses using a continuous flow-through reactor to measure the leaching during the first 30 min of fluid contact [25,27,28,31]. Feeding the test solution continuously through a glass particle bed affected the ion release and glass dissolution rates less than in static conditions. MA compositions suggested reduced ion release compared to single alkali glass [28]. However, the ion release kinetics from MA glasses at prolonged tests is still unclear.

This work explores the impact of K_2O for Na_2O substitution on the physical properties of bioactive glass S53P4, focusing on structural, sintering properties and bioactivity. Static and dynamic dissolution in TRIS-buffer and SBF were carried out to understand better the impact of MA composition on the ion dissolution kinetics. TRIS-buffer solution was selected to gain a more general understanding of glass dissolution without the impact of extensive calcium phosphate precipitation on the glass surface. At the same time, SBF provides similar alternate layer development as *in vivo*, especially in the dynamic flow environment used in this study. The results provide tools for tailoring new glass compositions for future clinical applications.

2. Materials and methods

2.1. Glass melting

Six glasses, with the nominal compositions given in Table 1, were melted (in-house using the traditional melt-quenching method). The batches consisted of analytical grades of Na_2CO_3, K_2CO_3, $CaCO_3$, $CaHPO_4{\cdot}2(H_2O)$, and Belgian quartz sand as the SiO_2 raw material. The glasses were melted in a Pt crucible at 1360 °C for 3 h, cast, annealed at 520 °C for 1 h, and then crushed. The glasses were remelted to ensure homogeneity. The annealed glass bars were crushed and sieved to give a particle size fraction of 300–500 μm. For future characterisations, the particles were washed with acetone at least three times to remove adhered powder and dried overnight at 40 °C.

Table 1
Nominal compositions of the experimental glasses.

Glass	Oxide content, mol.% (wt.%)				
	SiO_2	CaO	P_2O_5	Na_2O	K_2O
S53P4	53.9 (53.0)	21.8 (20.0)	1.7 (4.0)	22.7 (23.0)	–
5K	53.9 (51.6)	21.8 (19.5)	1.7 (3.8)	17.7 (17.5)	5.0 (7.5)
10K	53.9 (50.4)	21.8 (19.0)	1.7 (3.8)	12.7 (12.2)	10.0 (14.6)
15K	53.9 (49.2)	21.8 (18.6)	1.7 (3.7)	7.7 (7.2)	15.0 (21.5)
20K	53.9 (48.0)	21.8 (18.1)	1.7 (3.6)	2.7 (2.4)	20.0 (27.9)
22.7K	53.9 (47.3)	21.8 (17.9)	1.7 (3.5)	–	22.7 (31.3)

2.2. Characterisation of glasses

2.2.1. Glass and oxygen packing density

The density of glasses (ρ_{glass}) was measured in deionised water by Archimedes's principle. Oxygen parking density (ρ_{ox}) was calculated by dividing the oxygen atom mass in 1 mol of glass by the glass molar volume V_m:

$$\rho_{ox} = M_o / V_m = M_o \cdot \left(2x_{SiO_2} + 5x_{P_2O_5} + x_{CaO} + x_{Na_2O} + x_{K_2O}\right) / V_m \quad (1)$$

where M_o is the oxygen atomic weight, and x is the molar fractions of oxides. V_m was calculated by dividing the mass of 1 mol of glass divided by the measured density value (ρ_{glass}). Brauer et al. and Ray [27,36] have reported the detailed principle for oxygen packing density calculations.

2.2.2. Structure and phase composition

The glass powders were characterised using Fourier-transform infrared spectroscopy (FTIR) with a Harrick's Video-MVP™ ATR accessory. The ATR accessory was attached to a Bruker IFS 66S spectrometer equipped with a DTGS detector. The obtained spectra were collected for the range 4000 to 400 cm^{-1} with a resolution of 4 cm^{-1}. The FTIR spectra were measured for the as-prepared glasses and the samples after static and dynamic dissolution in SBF.

The amorphous nature of glasses was verified using X-ray diffraction (XRD, Empyrean Malvern Panalytical, Almelo, Netherlands) with the radiation source α-line of Cu radiation with the step size 2.0°/min at 40 mA, 40 kV, 2Θ range from 10° to 70°.

2.2.3. Thermal properties

The thermal properties indicating the glass transition temperature T_g and crystallisation peak temperature T_p were determined using differential scanning calorimetry, DSC (Netzsch STA 449F1). Fine powder (45 μm) of glasses was heated in a platinum pan in an N_2 atmosphere to 1300 °C with a heating rate of 10 °C/min.

The sintering behaviour of the glasses was studied using a heating microscope, HSM (Misura 3.0, Expert System). A cylindrical sample with a height of 3 mm and diameter of 2 mm was pressed from the glass powder (<45 μm). The sample was heated with a heating rate of 40 °C/min to 450 °C and imaged after every 5 °C increase.

2.2.4. In vitro dissolution

Dissolution tests were carried out for five glasses (S53P4, 5K, 10K, 15K, and 22.7K) with a particle size fraction of 300–500 μm in static and dynamic conditions. Two buffered solutions, a 50 mM TRIS and standard SBF, were used for the dissolution experiments. The pH of TRIS (pKa = 8.6 at 25 °C) was adjusted to 7.4 (at 37 °C) using 1 M HCl. SBF was prepared according to the instructions by Kokubo et al. [37]. Static dissolution tests were carried out up to 168 h at 37 °C using a surface area to volume ratio (SA/V) of 0.4 cm^{-1}. The surface area of glasses with a mean diameter of 400 μm was based on the density values, the volume of glass particles, and the estimated number of glass particles in 200–220 mg of glass sample. The polypropylene containers containing

glass particles in 30 ml of solution were placed in a shaking incubator agitated at 100 rpm. For static and dynamic dissolution tests, the mass of the sample varied from 200 to 220 mg depending on the glass composition to maintain constant molar ratios of alkali oxides. The higher the K_2O content, the higher the mass of the glass particles used for dissolution tests. Dynamic dissolution experiments were performed in a continuous flow-through reactor set-up developed by Fagerlund et al. [38]. The buffer solutions were fed through the glass particles using a flow rate of 0.2 ml min^{-1} for laminar flow conditions. This flow rate was assumed to provide appropriate information on bioactive glass dissolution *in vitro* and *in vivo* [39,40]. The total solution volume fed through the particle beds during the 72 h experiment was 864 ml. 4 ml of the solution was collected for 20 min after the reactor for the pH measurement and analysis of the ion concentration at several time points. Ion concentrations were determined using inductively coupled plasma atomic emission spectroscopy (ICP-OES) (Optima 5300 DV, PerkinElmer). The ion concentrations were analysed using the emission lines for Si ($\lambda = 251.611$ nm), Na ($\lambda = 589.592$ nm), Ca ($\lambda = 317.933$ nm), and P ($\lambda = 213.617$ nm). The solutions were diluted in the volume ratio 1:10 before ICP-OES analysis. The calibration procedure for the ICP-OES was done using ultrapure water and a commercial multi-element standard (Spectrascan) with 1, 5, and 20 ppm Si, Ca, Na, K, and P. After selected dissolution times, the glass particles were collected, washed with ethanol and dried overnight at 40 °C. The reaction layers at the particle surfaces were analysed using scanning electron microscopy (SEM, Leo 1530, Oberkochen, Germany) and energy-dispersive X-ray spectroscopy (EDX, Thermo Scientific UltraDry, Thermo Scientific, Madison WI).

3. Results

3.1. Structure and density

The XRD patterns in Fig. 1a verify the amorphous structure of the as-prepared glasses. FTIR spectra indicated the typical features of silicate glasses (Fig. 1b). The main absorption peaks between 860 and 1060 cm^{-1} are attributed to the Si–O–Si stretching mode: the bands between 860 and 960 cm^{-1} indicate non-bridging oxygens (NBO), and between 960 and 1000 cm^{-1} bridging oxygen (BO) [41]. As expected, substituting K_2O for Na_2O did not change the amorphous nature of the glasses or the network units.

The structural properties of the glasses can be estimated from the nominal composition and network connectivity (NC). The NC provides a basis for estimating *in vitro* bioactivity, glass transition temperature and crystallisation tendency [42]. In this work, K_2O was substituted for equal molar amounts of Na_2O. The NC was 2.54 for all glasses.

The densities of the glasses are given in Fig. 2a. The measured density of S53P4 was 2.66 ± 0.1 g/cm^3, as reported elsewhere [43]. The density of the glasses decreased linearly with increasing K_2O substitution to 2.51 g/cm^3. A simple substitution of heavier K_2O for Na_2O would suggest increased density. However, the opposite trend can be explained by changes in the molar volume of the glasses. The pronounced increase in the calculated molar volume (Fig. 2b) inversely correlates with the decrease in the oxygen packing density with increasing substitution of the larger potassium for sodium.

3.2. Thermal properties

The thermal properties of the glasses were characterised using DSC. The endothermic peaks in the DSC curves (Fig. 3a) give the glass transition temperatures (T_g). S53P4 composition presented as a reference. The T_g values of all glasses are plotted against the mol.% of K_2O in Fig. 4a. The glasses containing K_2O indicated higher T_g values than those containing only Na_2O: T_g increased from 540 °C for S53P4 to 668 °C for 22.7K with K_2O only. The crystallisation peak temperature (T_p) was identified only for glasses containing up to 15 mol.% of K_2O. Interestingly, T_p was slightly lower for the glass with 5% K_2O than for S53P4 (740 compared to 755 °C). For other glasses, T_p increased significantly with increasing K_2O share: 846, 954, and 1010 °C for 15, 20, and 22.7% K_2O, respectively.

The sintering behaviour of fine-grained glass powders was investigated using HSM (Fig. 3b). The sintering temperature (T_{si}) is defined in standard DIN51730 as the shrinkage of the initial sample height to 95% [25]. Fig. 4a summarises the T_{si} values. For 5K, the T_{si} deviated from the linearity by giving the lowest value (615 °C). The crystallisation onset temperature, T_{xi}, corresponds to the starting temperature of the plateau, i.e., constant sample height, after the first temperature decrease. T_{xi} as a function of K_2O substitution is given in Fig. 4a. A slight reduction was observed for 5K, after which the crystallisation onset temperature increased with increasing K_2O share to 894 °C for 22.7 mol.%.

The hot-working range, given as the difference between the onset crystallisation temperature on HSM curves and glass transition temperature on DSC, $\Delta T = T_{xi} - T_g$, significantly increased with K_2O substitution from 115 °C for S53P4 to 226 °C for 22.7K (Fig. 4b). The difference between glasses 20K and 22.7K was minor. The results suggest that replacing around 20% of Na_2O with K_2O leads to the narrowest processing window between T_g and T_{xi} (105 °C).

3.3. Static in vitro dissolution

Fig. 5 shows the results from the static dissolution experiments. Ion concentrations are given in mmol/L and as the dissolved fraction, describing the extent to which ions in the original glass had dissolved and were analysed in the solution. The pH changes and ion concentrations in static TRIS at 24, 72, and 168 h are shown in Fig. 5 a, c, and e. The dissolution of glasses led to a typical pH increase with increasing K_2O substitution up to 7.75 at 168 h. The pH at 24 and 72 h (Fig. 5 a and c) increased gradually with the potassium content up to 15K (24 h: pH=7.52±0.01, 72 h: pH=7.63±0.01), while for 22.7K, slight decreases

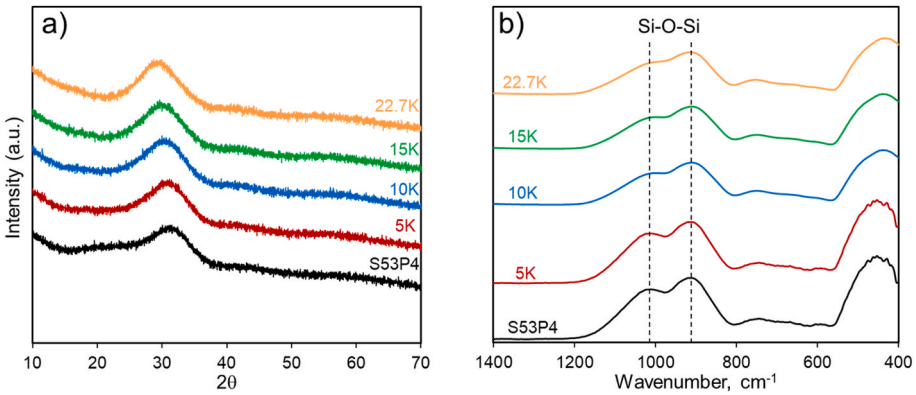

Fig. 1. XRD patterns (a) and FTIR spectra (b) of the experimental glasses.

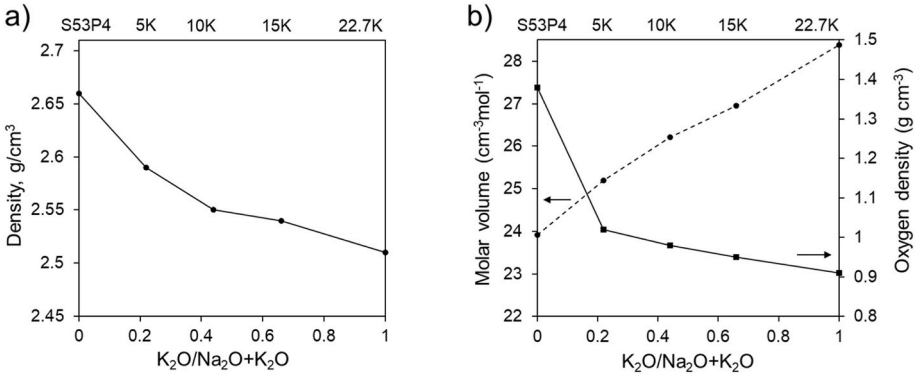

Fig. 2. (a) Density, (b) molar volume (left axis), and oxygen packing density (right axis) versus K_2O for Na_2O substitution in the glass. The lower x-axes give the molar potassium substitution percentage, and the upper axes give the glass codes.

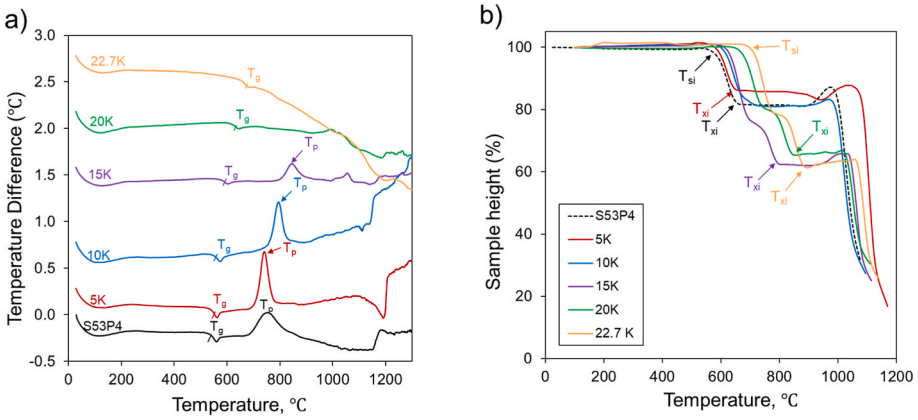

Fig. 3. DSC (a) and HSM (b) curves for the investigated glasses.

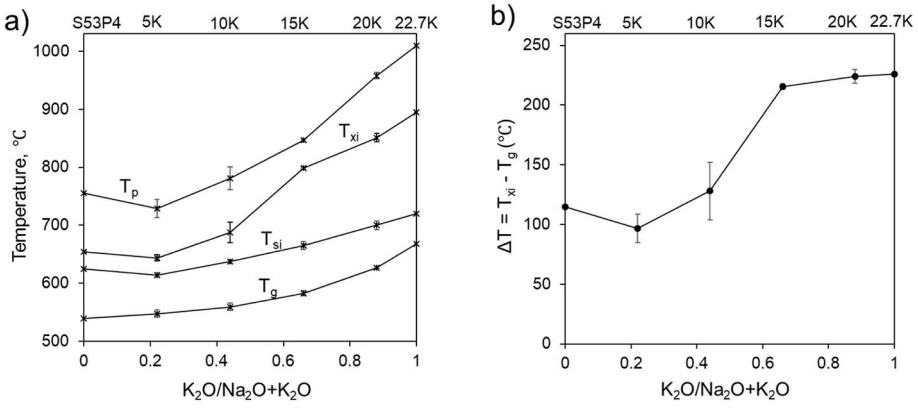

Fig. 4. Thermal properties of the produced glasses: a) glass transition temperature T_g, crystallisation temperature T_p, sintering temperature T_{si}, the onset of crystallisation temperature T_{xi}, and b) hot working range.

were measured. At the longest time point, 168 h, the maximum pH increase of 7.74±0.01 was seen for 22.7K, while the other single alkali S53P4 gave the lowest value (pH = 7.7).

The ion dissolution trends of the MA glasses were in line with the solution pH changes (Fig. 5 a, c, and e). At shorter times, the dissolution suggested maximum values of total alkalis, calcium, and silicon species for 15K. The dissolution became more linear with prolonged time, suggesting minor increases of Si and Ca, while the alkali release (Na+K) was almost constant at 168 h (Fig. 5e).

Fig. 5 b, d, and f show the dissolved ion fractions in static TRIS. Interestingly, the relative release of all ions showed maximum values for 15K at 24 h. However, the non-linear trends in dissolved fractions between the glasses with different K_2O contents decreased with increasing time and were non-linear only for total alkalis at 168 h (Fig. 5f). The dissolved fractions suggested an increasing trend with increasing K_2O content in the glass for all species.

3.4. Dynamic dissolution in TRIS and SBF

Ion concentrations released from the glasses into TRIS at 4, 24, and 72 h of dynamic dissolution are shown in Fig. 6. The overall ion dissolution decreased with time. At 4 and 24 h, the total release of Na+K

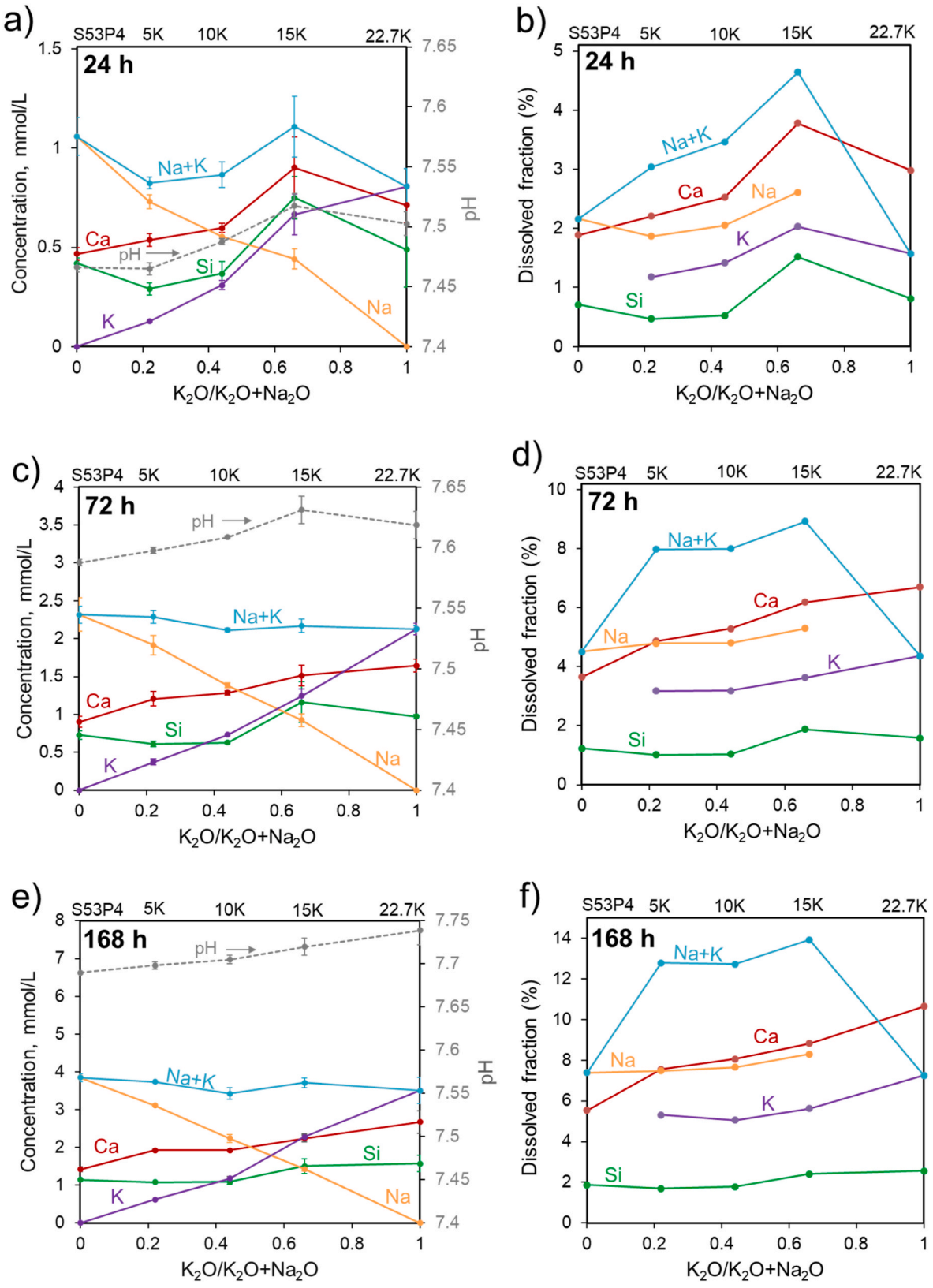

Fig. 5. Average ion concentrations (mmol/L) (a, c, e) and dissolved fraction of ions (b, d, f) at 24, 72, 168 h of static immersion in TRIS.

showed similar nonlinear changes as the solution pH with increasing K_2O content. At the longest dissolution time, 72 h, the pH gradually increased with K_2O substitution. A similar trend was measured for the Si release. Ca ions in the solution suggested a minor increase with increasing K_2O content at all time points.

The concentrations of Si species and the pH changes in dynamic SBF are shown as functions of K_2O at several time points in Fig. 7. As the as-prepared SBF contains ions of Na, Ca, and P but no Si, the Si release was

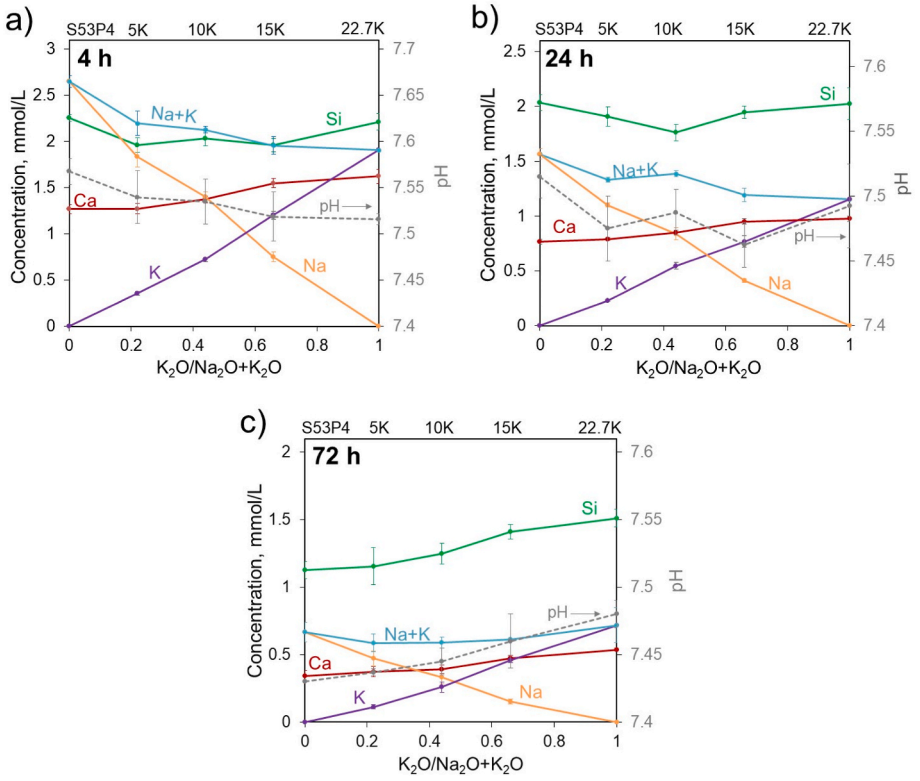

Fig. 6. Average ion concentrations (mmol/L) and pH as functions of K_2O content in the glass after dynamic dissolution in TRIS a) 4 h, b) 24 h, and c) 72 h.

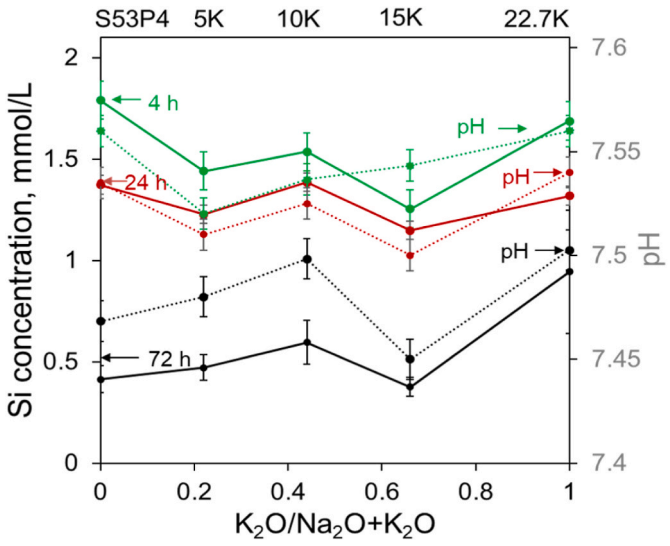

Fig. 7. pH and average ion concentrations of Si (mmol/L) and pH as functions of K_2O content in the glass after dynamic dissolution in SBF at 4, 24, and 72 h.

assumed to provide indications of the overall durability and dissolution mechanisms of the MA glasses in dynamic flow conditions. The highest Si concentrations were analysed at 4 h. Interestingly, the changes in Si concentration showed a similar nonlinear composition dependence as in the static system at 4 and 24 h. The nonlinearity in Si released with increasing K_2O was also measured at 72 h. The pH changes were similar to the Si concentrations released from the MA glasses at all time points. Except for 15K, Si release and pH increase almost linearly with K_2O content in the glass.

3.5. *In vitro bioactivity: reaction layers*

Fig. 8 shows SEM images and EDX analyses of the cross-sections of glass particles after 168 h of static dissolution in TRIS and SBF. All glasses had a SiO_2-rich layer, a dark grey layer next to the bulk glass in the images. The SEM images revealed no distinct calcium phosphate (CaP) layer, typically seen as a white outer layer. The SiO_2-rich layer was thickest (15–20 μm) for 15K. The layer thickness varied between 10 and 15 μm for the other K-containing glasses. A mixed SiO_2+CaP layer was detected on some particles of S53P4, 5K, and 15K. After static dissolution in SBF, all glasses indicated good bioactivity, i.e., a distinct SiO_2-rich and a CaP layer with a Ca/P ratio typical for hydroxyapatite. However, 5K showed a less developed SiO_2-rich and a thin mixed SiO_2+CaP layer on some particles. S53P4 and 10K had well-developed CaP surface layers, while CaP was identified only on some particles of the glasses with the highest K_2O contents.

Fig. 9 shows SEM images of particle cross-sections after 72 h of dynamic dissolution in TRIS and SBF. SiO_2-rich layer was identified at all MA glasses after the dissolution in TRIS. For 15K, the layer was seen only on some particles. The thickest SiO_2 layers of up to 32 μm were identified on the glasses containing one alkali only, i.e., S53P4 and 22.7K. Uneven CaP layer was seen on S53P4 particles, while a mixed SiO_2+CaP layer can be noticed on some particles of 22.7K after the dissolution in TRIS.

After 72 h of continuous flow in SBF, all glasses indicated more developed and thicker reaction layers than after 168 h of static dissolution. 22.7K particles had the thickest SiO_2-rich layer, 20–32 μm, and CaP layers, 10–25 μm. The SEM-EDX analyses verified CaP on the MA glass 10K and single-alkali glasses (S53P4 and 22.7K). A mixed SiO_2+-CaP layer was identified locally on some 15K particles.

Fig. 10 gives the FTIR spectra of the glasses after 72 h of dynamic (a) and 168 h of static (b) dissolution in SBF. FTIR spectra of all glasses exhibited vibrations at 605 cm^{-1} after static dissolution in SBF. This single peak corresponds to the formation of amorphous calcium phosphate (ACP), which is usually taken as an indication of the presence of

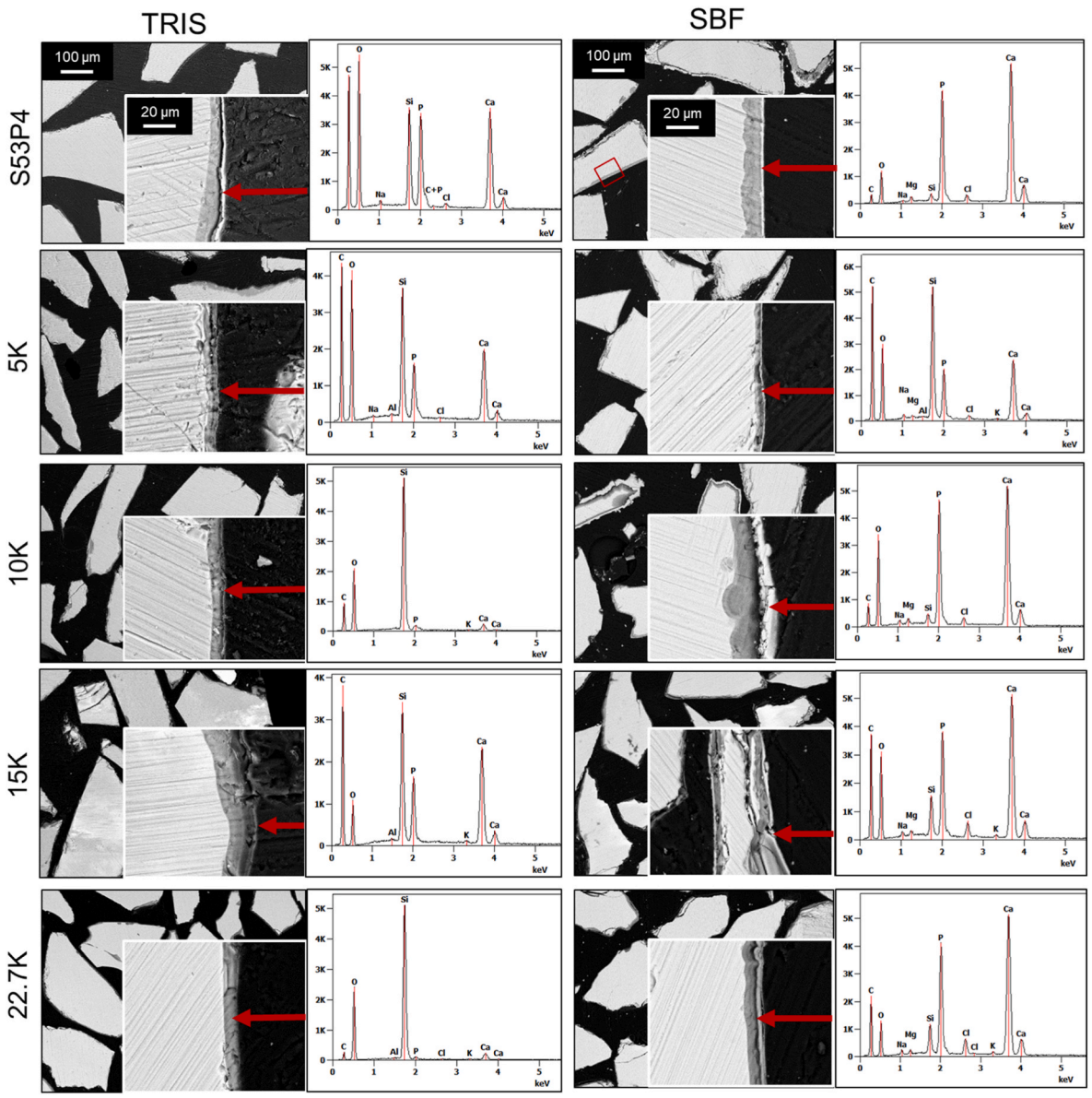

Fig. 8. SEM images of S53P4 and MA glass particles in two magnifications after 168 h of static dissolution in TRIS and SBF. The arrow shows the location of the area for the EDX spectrum.

precursors to hydroxyapatite (HA). However, the additional band at 560–565 cm^{-1} related to the phosphate groups, was detected only for S53P4 and 22.7K after the dynamic dissolution in SBF. These bands (560–565 cm^{-1} and 605 cm^{-1}) represent asymmetric bending vibrations of PO_4^{3-}, indicating the formation of HA [27]. After 168 h in static SBF, only the band at 605 cm^{-1} was clearly seen for all glasses except for 5K. The spectra imply that the rate of apatite formation decreased for the MA glasses.

4. Discussion

Although potassium has a higher molar mass than sodium, the density decreased with increasing K_2O substitution for Na_2O in S53P4 (Fig. 2a). The density decrease can be explained by the expansion of the glass network, which is caused by the larger ionic radius of K^+ (138 ppm) compared to Na^+ (102 ppm) [25,27,28]. A similar decreasing trend in glass density has been reported for 45S5 with increasing K_2O substation for Na_2O [21,25–28]. The difference in the ionic radius between Na^+ and K^+ affects the molar volume and oxygen packing density. Therefore, the density change can be described by increasing the molar volume and decreasing the oxygen packing density of the glasses (Fig. 2b). Thus, substituting K_2O for Na_2O affected the glass network, making potassium-rich glasses less compact than sodium-rich glasses [21,25,27–31]. The oxygen density of the experimental glasses correlated with the density change trends, as suggested for glasses with a constant NC [42].

Substituting potassium for sodium also affected the thermal properties. The increase in the glass transition temperature T_g (Fig. 4a) can be explained by the smaller ion radius and the higher sodium field strength than potassium [36,44]. Ray pointed out that the influence of field strength may depend on the polymerisation degree of the glass network and is relevant mainly for alkali silicate glasses [36]. Avramov et al. reported a similar increase in T_g with increasing K_2O substitution for Na_2O for the bioactive glass 45S5 [24]. They found that T_g increases almost linearly with the alkali cation radius due to a spatial hindrance. The larger ionic radius of K^+ compared to Na^+ provides higher spatial hindrance on the mobility of the modified tetrahedra (SiO_4) containing NBO. Tylkowski and Brauer reported the MAE of T_g for 45S5 when

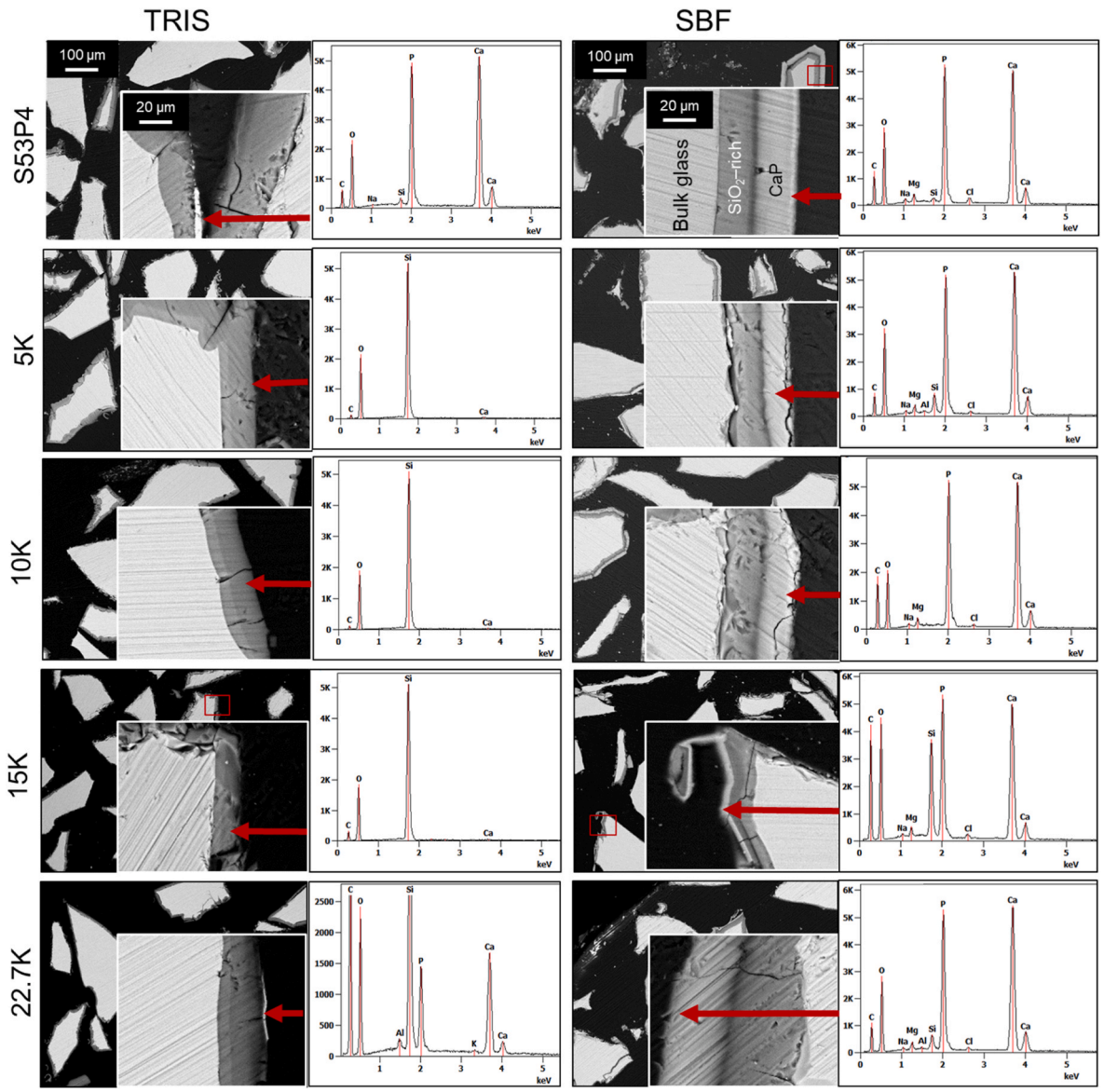

Fig. 9. SEM images of S53P4 and MA glass particles in two magnifications after 72 h of dynamic dissolution in TRIS and SBF. The arrow shows the location of the area for the EDX spectrum.

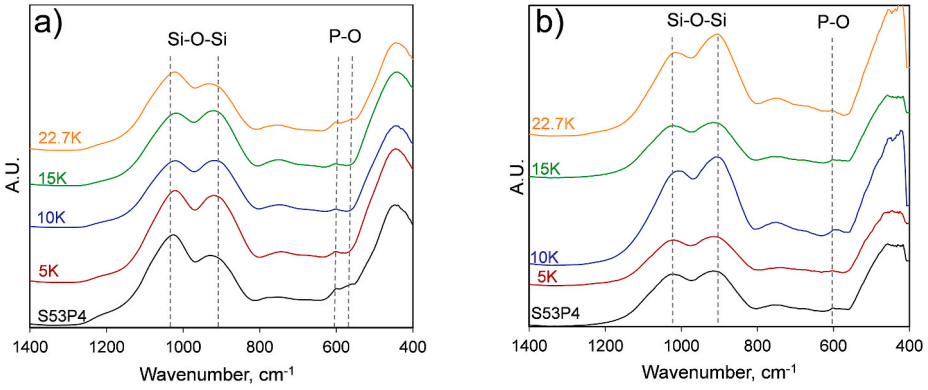

Fig. 10. FTIR spectra of glasses after 72 h of dynamic (a) and 168 h of static (b) dissolution in SBF.

replacing 20–50% of Na_2O with K_2O [21]. However, they did not note a similar decrease in crystallisation temperature, but the processing window increased almost linearly with increasing substitution. A slight reduction of T_p (Fig. 4a) for 5K is similar to several published studies for other silicate-based bioactive glasses with a small share of K_2O [21,25,29]. The increase in crystallisation temperatures for the MA

compositions resulted in a significantly improved processing window when substituting K_2O for Na_2O in 45S5 [21]. In the present work, the processing window increased at higher substitutions than 5%, i.e., for glasses 10K–22.7K. Therefore, substituting K_2O for Na_2O suggested MAE for the 5K glass by showing deviation from the linearity. Similar findings have been found by Wang et al. [25]. The substitution of K_2O for Na_2O can be used to prevent the crystallisation of glasses and also may help to control the glass dissolution in the body environment [6,30].

Static dissolution studies in TRIS-buffer were carried out to understand better the ion release from MA glasses. MAE has been reported for glasses in static aqueous solutions with a pH lower than 9 [45]. In this work, alkali ions were released into TRIS through a typical ion-exchange reaction between protons in the solution, with a simultaneous increase in the pH. As the pH stayed well below 9, MAE could be possible. Substituting one alkali oxide for another in compositions typical for bioactive silicate glasses has not been reported to provide any distinct MAE in static or dynamic buffered solutions [25,27,28]. In contrast, MAE became evident for compositions with a higher SiO_2 content [25]. In this work, the ion release from the glass network indicated incongruent dissolution, showing less Si release than modified ions (Fig. 5). At 24 h, glass 15K showed some indications of MAE by giving higher pH and ion concentrations of all ions. Brauer et al. studied alkali released from two alkali-modified compositions of 45S5, where Na_2O was replaced with a Li_2O–K_2O mixture [27]. They reported that the total alkali (Li+K) release slightly decreased with increasing potassium content at 24 h of static immersion, although the ionic radius of Li^+ (76 p.m.) is significantly less compared to K^+ (138 p.m.). No MAE was reported in the static buffer solution. Their experiments were done using the same mass of glasses, although the difference in the molar masses of Li and K is large. Thus, the trends cannot be directly compared for the total molar alkali ion contents in the glasses. In this work, the release of calcium ions increased simultaneously with the increasing potassium content. Several studies have reported similar findings [22,25,28,29]. The fast Ca release with more ionic bonds cannot be related to the electronegativity of the alkali metal ion or the character of the M−O bond. In contrast, Ca ion release has been explained by the compactness of the silicate glass network via modifier ionic radius [28]. The fast release of network modifying ions (Na + K, Ca) and high dissolved ion fractions of 15K at 24 h (Fig. 5a and b) may influence the electric activity of nerve and muscle cells [44,46]. Moreover, the high fractions of sodium and potassium released from 15K at all time points in static immersion (Fig. 5) can be explained by the large size of potassium providing a less tightly packed glass network than in the sodium-rich glasses [36].

The constant solution flow in the dynamic flow-through experiments enables measuring the ion release without possible solution saturation [38]. The dynamic dissolution patterns have been related to *in vivo* bioactivity of glasses [47]. Initial dynamic dissolution (first 20 min) in both solutions indicated the highest pH for 5K (7.82 in TRIS and 7.75 in SBF), followed by a decrease at prolonger dissolution. The larger ionic radius and higher ion mobility of potassium within the expanded glass network make it more accessible for H^+ diffusion in the ion-exchange reaction. Potassium has weaker bonding to the glass network compared to sodium. Thus, the release of this modifier ion occurs easier [28,31]. The first reactions between the solution and bioactive glasses are accompanied by the ion-exchange reaction with the increase of solutions' pH followed by the initial release of Si species, precipitation and formation of a SiO_2-rich surface layer by condensation of Si–OH groups [46]. The pH in dynamic TRIS gradually decreased with increasing content of K_2O in the glasses at 4 and 24 h. These pH changes followed the release of total alkalis from the glasses. The decreasing pH values and ion release have been explained by decreasing mass of samples left and differences in the underlying ion transport mechanism in the presence of two different alkali ions [45]. As the ion release is affected by the packing of the silicate network, the differences in the ion transport mechanism correlate with the glass structure [28]. MAE tends to affect the release of ions from silicate-based glasses by showing less pronounced pH changes for the glasses containing sodium and potassium compared to those with only one alkali oxide [48]. Interestingly, at the longest time point, 72 h, the pH increased with K_2O substitution and correlated with the release of Si species. The solubility of Si species strongly depends on pH [49]. Small silicate units may be released without hydrolysis of Si–O–Si from the highly disrupted structure of bioactive glass, such as 45S5 [10,48]. However, S53P4 with a more cross-linked structure has also been reported to degrade entirely *in vivo* [50,51]. Therefore, Si–O–Si hydrolysis occurs, caused by a pH increase at the glass/solution interface [42,52]. The glasses with a more polymerised network structure may result in lower concentrations of modifier ions due to the ion exchange near the surface of glass particles [28].

The *in vitro* bioactivity of the investigated glasses was studied using TRIS and SBF in static and dynamic conditions. The formation of reaction layers strongly depended on the particle size, glass composition, local environment around the particles, and solution composition [31]. TRIS can form soluble complexes with calcium ions which might interfere with the precipitation of CaP [53]. The absence of CaP for the MA compositions in dynamic TRIS dissolution can be explained by the low concentration of P species released into the solution. Minor differences in the reaction layer structures may have been affected by uneven exposure of glass particles in the container depending on their location in the particle bed [32,54]. However, as the sample mass was limited, the differences in the layer development between the individual particles were insignificant (Fig. 9). For a larger particle bed, more distinct differences are likely [32]. A high solution pH enhances the CaP precipitation due to changes in the supersaturation level as a function of pH [33]. Interestingly, in this work, the highest pH (7.74 ± 0.02) was seen for 10K at 168 h of static SBF (the trend is not shown here) with a more developed CaP layer than on the other glasses (Fig. 8). However, the peak attributed to the vibrations of PO_4^{3-} at 560 cm^{-1} was not confirmed in the FTIR spectra (Fig. 10b) for 10K. Similar results were reported by Crovace et al., who studied in static SBF the reactions of potassium-substituted bioactive glasses 45S5 [29]. Their results implied similar HCA formation ability in SBF for all compositions but enhanced matrix mineralisation in cell culture studies for the glasses containing 12.2 mol.% Na_2O and 12.2 mol.% K_2O or 18.3 mol.% Na_2O and 6.1 mol.% K_2O compared to the single-alkali compositions. The increase in extracellular K^+ in the cell culture was assumed to inhibit the efflux of intracellular K^+, leading to the stimulation of osteoblastic cell proliferation [29]. However, high potassium release into the interfacial solution might have an unfavourable effect on the cellular processes [55].

Although the NC of experimental glasses was the same, the difference in bioactivity could be attributed to the ion dissolution kinetics. Atila et al. reported that partial substitution of K_2O for Na_2O in 45S5 bioactive glass affected the diffusion coefficient and activation energies, i.e., 45S5 provided optimal ion release kinetics and faster apatite formation than the MA glasses [30]. According to their findings, the fully substituted potassium glass, K–45S5, represented higher *in vitro* bioactivity than the corresponding lithium-substituted glass, Li–45S5. In this work, glass 15K had the least developed CaP layer after 72 h in dynamic SBF (Fig. 9). This also was seen as the lowest concentration of Si species and lower pH changes than for the other glasses. The reduced rates of CaP layer formation for potassium-substituted glasses can be related to incorporating Na^+ and K^+ into the apatite lattice. Due to the larger ionic radius of potassium, the rate of CaP layer formation may result in reduced apatite crystallisation of mixed sodium-potassium glasses [56]. Both single-alkali glasses (S53P4 and 22.7K) had thicker reaction layers indicating higher bioactivity than the MA glasses after dynamic dissolution in SBF (Figs. 9 and 10). The large difference in the solution volume in contact with the glasses in the static and dynamic was assumed to affect the differences in the reaction layer thicknesses seen after 168 h (static) and 72 h (dynamic). The thinner reaction layers in the static conditions likely depended on the limited diffusion of the released species caused by the high ion concentrations in the interfacial solution.

In contrast, ions were not saturated in the interfacial solution in the dynamic condition, thus enabling faster release and diffusion of the ions.

5. Conclusions

Substituting K_2O for Na_2O in bioactive glass S53P4 influenced the physical properties, ion release and reaction layer formation. The density of the glasses decreased with increasing K_2O substitution due to the expanded glass network. A mixed-alkali effect was observed for high-temperature properties. The effect was highest for the composition with around 20% replacement of Na_2O with K_2O, giving lower temperatures for sintering and crystallisation, leading to the narrowest hot-working range. In static conditions, the highest fractions of dissolved ions in the TRIS-buffer were analysed for S53P4 composition, in which around 66% of Na_2O was replaced with K_2O at 24 h. However, the dissolved ion fraction slightly increased with the K_2O content at prolonged dissolution. Similar trends were observed in dynamic dissolution in the TRIS-buffer. The release of Si species increased almost linearly with increasing K_2O substitution at longer times. The release of Si species was lowest at all measured time points for the glass in which 66% of Na_2O was replaced with K_2O (15K composition) in dynamic simulated body fluid. Reaction layers formation ability was higher for the single-alkali glasses than the mixed-alkali glasses. In general, the results suggest that <40% substitutions of N_2O with K_2O decrease the thermal processing window and the bioactivity of glass S53P4. However, the thermal processing window markedly increases at higher substitutions, while the *in vitro* bioactivity is less than for single-alkali compositions. The composition with only K_2O had a low tendency to crystallise and promising *in vitro* bioactivity.

Declaration of competing interest

The authors declare that they have no known competing financial interests or personal relationships that could have appeared to influence the work reported in this paper.

Acknowledgments

This work was supported by the Academy of Finland (project 341405). Linus Silvander, Luis Bezerra, Peter Backman, and Jaana Paananen are acknowledged for their technical assistance with SEM-EDX, ICP-OES, XRD, DSC, and HSM measurements.

References

[1] L.L. Hench, R.J. Splinter, W.C. Allen, T.K. Greenlee, Bonding mechanisms at the interface of ceramic prosthetic materials, J. Biomed. Mater. Res. 5 (1971) 117–141, https://doi.org/10.1002/jbm.820050611.
[2] L.L. Hench, The story of bioglass, J. Mater. Sci. Mater. Med. 17 (2006) 967–978, https://doi.org/10.1007/s10856-006-0432-z.
[3] J.R. Jones, Review of bioactive glass: from Hench to hybrids, Acta Biomater. 9 (2013) 4457, https://doi.org/10.1016/j.actbio.2012.08.023.
[4] S. Fagerlund, J. Massera, N. Moritz, L. Hupa, M. Hupa, Phase composition and in vitro bioactivity of porous implants made of bioactive glass S53P4, Acta Biomater. 8 (2012) 2331–2339, https://doi.org/10.1016/j.actbio.2012.03.011.
[5] M. Brink, The influence of alkali and alkaline earth on the working range for bioactive glasses, J. Biomed. Mater. Res. 36 (1997) 109–117, https://doi.org/10.1002/(sici)1097-4636(199707)36:1<109::aid-jbm13>3.0.co;2-d.
[6] M. Brink, T. Turunen, R.P. Happonen, A. Yli-Urpo, Compositional dependence of bioactivity of glasses in the system Na_2O-K_2O-MgO-CaO-B_2O_3-P_2O_5-SiO_2, J. Biomed. Mater. Res. 37 (1997) 114–121, https://doi.org/10.1002/(sici)1097-4636(199710)37:1<114::aid-jbm14>3.0.co;2-g.
[7] H. Arstila, E. Vedel, L. Hupa, M. Hupa, Predicting physical and chemical properties of bioactive glasses from chemical composition. Part 2: devitrification characteristics, Glass Technol. Part A 49 (2008) 260–265.
[8] M. Brink, K. Karlsson, A. Yli-Urpo, Bioactive Glasses and Their Use, 1996. Patent number WO96/21628 (US6054400A).
[9] M.N. Rahaman, D.E. Day, B.S. Bal, Q. Fu, S.B. Jung, L.F. Bonewald, A.P. Tomsia, Bioactive glass in tissue engineering, Acta Biomater. 7 (2011) 2355–2373, https://doi.org/10.1016/j.actbio.2011.03.016.
[10] R.G. Hill, D.S. Brauer, Predicting the bioactivity of glasses using the network connectivity of split network models, J. Non-Cryst. Solids 357 (2011) 3884, https://doi.org/10.1016/j.jnoncrysol.2011.07.025.
[11] A. Itälä, J. Koort, H.O. Ylänen, M. Hupa, H.T. Aro, Biologic significance of surface microroughing in bone incorporation of porous bioactive glass implants, J. Biomed. Mater. Res. A67 (2003) 496–503, https://doi.org/10.1002/jbm.a.10501.
[12] Q. Fu, M.N. Rahaman, B.S. Bal, R.F. Brown, D.E. Day, Mechanical and *in vitro* performance of 13-93 bioactive glass scaffolds prepared by a foam replication technique, Acta Biomater. 4 (2008) 1854–1864, https://doi.org/10.1016/j.actbio.2008.04.019.
[13] X. Liu, M.N. Rahaman, Q. Fu, Oriented bioactive glass (13-93) scaffolds with controllable pore size by unidirectional freezing of camphene-based suspensions: microstructure and mechanical response, Acta Biomater. 7 (2011) 406–416, https://doi.org/10.1016/j.actbio.2010.08.025.
[14] X. Liu, M.N. Rahaman, Q. Fu, A.P. Tomsia, Porous and strong bioactive glass (13-93) scaffolds prepared by unidirectional freezing of camphene-based suspensions, Acta Biomater. 8 (2012) 415–423, https://doi.org/10.1016/j.actbio.2011.07.034.
[15] K.C.R. Kolan, M.C. Leu, G.E. Hilmas, R.F. Brown, M. Velez, Fabrication of 13-93 bioactive glass scaffolds for bone tissue engineering using direct selective laser sintering, Biofabrication 3 (2011), 025004, https://doi.org/10.1088/1758-5082/3/2/025004.
[16] N.D. Doiphode, T. Huang, M.C. Leu, M.N. Rahaman, D.E. Day, Freeze extrusion fabrication of 13-93 bioactive glass scaffolds for bone repair, J. Mater. Sci. Mater. Med. 22 (2011) 515–523, https://doi.org/10.1007/s10856-011-4236-4.
[17] S. Eqtesadi, A. Motealleh, A. Pajares, P. Miranda, Effect of milling media on processing and performance of 13-93 bioactive glass scaffolds fabricated by robocasting, Ceram. Int. 41 (2015) 1379–1389, https://doi.org/10.1016/j.ceramint.2014.09.071.
[18] D. Bellucci, V. Cannillo, A. Sola, Calcium and potassium addition to facilitate the sintering of bioactive glasses, Mater. Lett. 65 (2011) 1825–1827, https://doi.org/10.1016/j.matlet.2011.03.060.
[19] E. Fiume, D.U. Tulyaganov, A. Akbarov, N. Ziyadullaeva, A. Cochis, A.C. Scalia, Biological evaluation of new sodium-potassium-silico-phosphate glass for bone regeneration: in vitro and in vivo studies, Materials 14 (2021) 4546, https://doi.org/10.3390/ma14164546.
[20] J.J. Alm, J.P.A. Frantzén, N. Moritz, P. Lankinen, M. Tukiainen, M. Kellomäki, H. T. Aro, In vivo testing of a biodegradable woven fabric made of bioactive glass fibers and PLGA80-A pilot study in the rabbit, J. Biomed. Mater. Res. Part B Appl. Biomater. 93 (2010) 573–580, https://doi.org/10.1002/jbm.b.31618.
[21] M. Tylkowski, D.S. Brauer, Mixed alkali effect in Bioglass® 45S5, J. Non-Cryst. Solids 376 (2013) 175–181, https://doi.org/10.1016/j.jnoncrysol.2013.05.039.
[22] D.E. Day, Mixed alkali glasses – their properties and uses, J. Non-Cryst. Solids 21 (1976) 343–372, https://doi.org/10.1016/0022-3093(76)90026-0.
[23] R.H. Doremus, Mixed alkali effect and interdiffusion of Na and K ions in glass, J. Am. Ceram. Soc. 57 (1974) 478–480, https://doi.org/10.1111/j.11512916.1974.tb11395.x.
[24] I. Avramov, T.S. Vassilev, I. Penkov, The glass transition temperature of silicate and borate glasses, J. Non-Cryst. Solids 351 (2005) 472–476, https://doi.org/10.1016/j.jnoncrysol.2005.01.044.
[25] X. Wang, S. Fagerlund, J. Massera, B. Södergård, L. Hupa, Do properties of bioactive glasses exhibit mixed alkali behaviour? J. Mater. Sci. 52 (2017) 8986–8997, https://doi.org/10.1007/s10853-017-0915-y.
[26] V. Cannillo, A. Sola, Potassium-based composition for a bioactive glass, Ceram. Int. 35 (2009) 3389–3393, https://doi.org/10.1016/j.ceramint.2009.06.011.
[27] D.S. Brauer, R. Brückner, M. Tylkowski, L. Hupa, Sodium-free mixed alkali bioactive glasses, Biomed. Glasses 2 (2016) 99–110, https://doi.org/10.1515/bglass-2016-0012.
[28] R. Brückner, M. Tylkowski, L. Hupa, D.S. Brauer, Controlling the ion release from mixed alkali bioactive glasses by varying modifier ionic radii and molar volume, J. Mater. Chem. B 4 (2016) 3121–3134, https://doi.org/10.1039/C5TB02426A.
[29] M.C. Crovace, V.O. Soares, A.C.M. Rodrigues, O. Peitl, L.M.S.C. Raucci, P.T. de O. Oliveira, E.D. Zanotto, Understanding the mixed alkali effect on the sinterability and *in vitro* performance of bioactive glasses, J. Eur. Ceram. Soc. 41 (2021) 4391–4405, https://doi.org/10.1016/j.jeurceramsoc.2020.11.020.
[30] A. Atila, Y. Ouldhnini, S. Ouaskit, A. Hasnaoui, Atomistic insights into the mixed-alkali effect in phosphosilicate glasses, Phys. Rev. B 105 (2022), 134101, https://doi.org/10.1103/PhysRevB.105.134101.
[31] L. Hupa, S. Fagerlund, J. Massera, L. Björkvik, Dissolution behaviour of bioactive glasses S53P4 when sodium is replaced by potassium, and calcium with magnesium or strontium, J. Non-Cryst. Solids 432 (2016) 41–46, https://doi.org/10.1016/j.jnoncrysol.2015.03.026.
[32] D. Zhang, M. Hupa, H.T. Aro, L. Hupa, Influence of fluid circulation on in vitro bioactivity of bioactive glass particles, Mater. Chem. Phys. 111 (2008) 497–502, https://doi.org/10.1016/j.matchemphys.2008.04.055.
[33] S. Fagerlund, L. Hupa, M. Hupa, Comparison of reactions of bioactive glasses in different aqueous solutions, Ceram. Trans. 218 (2010) 101–113, https://doi.org/10.1002/9780470909898.ch11.
[34] K. Schuhladen, X. Wang, L. Hupa, A.R. Boccaccini, Dissolution of borate and borosilicate bioactive glasses and the influence of ion (Zn, Cu) doping in different solutions, J. Non-Cryst. Solids 502 (2018) 22–34, https://doi.org/10.1016/j.jnoncrysol.2018.08.037.
[35] P. Sinitsyna, O. Karlström, L. Hupa, *In vitro* dissolution of bioactive glass S53P4 microspheres, J. Am. Ceram. Soc. 105 (2022) 1658–1670, https://doi.org/10.1111/jace.18014.

[36] N.H. Ray, Composition-property relationships in inorganic oxide glasses, J. Non-Cryst. Solids 15 (1974) 423–434, https://doi.org/10.1016/0022-3093(74)90148-3.
[37] T. Kokubo, H. Takadama, How useful is SBF in predicting *in vivo* bone bioactivity? Biomaterials 27 (2006) 2907–2915, https://doi.org/10.1016/j.biomaterials.2006.01.017.
[38] S. Fagerlund, P. Ek, L. Hupa, M. Hupa, Dissolution kinetics of a bioactive glass by continuous measurement, J. Am. Ceram. Soc. 95 (2012) 3130–3137, https://doi.org/10.1111/j.1551-2916.2012.05374.x.
[39] L. Aalto-Setälä, P. Uppstu, P. Sinitsyna, N.C. Lindfors, L. Hupa, Dissolution of amorphous S53P4 glass scaffolds in dynamic in vitro conditions, Materials 14 (2021) 4834, https://doi.org/10.3390/ma14174834.
[40] E. Eriksson, R. Björkenheim, G. Strömberg, M. Ainola, P. Uppstu, L. Aalto-Setälä, V.-M. Leino, L. Hupa, J. Pajarinen, N.C. Lindfors, S53P4 bioactive glass scaffolds induce BMP expression and integrative bone formation in a critical-sized diaphysis defect treated with a single-staged induced membrane technique, Acta Biomater. 126 (2021) 463–476, https://doi.org/10.1016/j.actbio.2021.03.035.
[41] J. Serra, P. González, S. Liste, S. Chiussi, B. León, M. Pérez-Amor, H.O. Ylänen, M. Hupa, Influence of the non-bringing oxygen groups on the bioactivity of silicate glasses, J. Mater. Sci. Mater. Med. 13 (2002) 1221–1225, https://doi.org/10.1023/A:1021174912802.
[42] D.S. Brauer, Bioactive glasses – structure and properties, Angew. Chem. Int. Ed. 54 (2015) 4160–4181, https://doi.org/10.1002/anie.201405310.
[43] A.L.B. Maçon, T.B. Kim, E.M. Valliant, K. Goetschius, R.K. Brow, D.E. Day, A. Hoppe, A.R. Boccaccini, Ill Yong Kim, C. Ohtsuki, T. Kokubo, A. Osaka, M. Vallet-Regí, D. Arcos, L. Fraile, A.J. Salinas, A.V. Teixeira, Yu Vueva, R. M. Almeida, M. Miola, C. Vitale-Brovarone, E. Verné, W. Höland, J.R. Jones, A unified in vitro evaluation for apatite-forming ability of bioactive glasses and their variants, J. Mater. Sci. Mater. Med. 26 (2015) 1–10, https://doi.org/10.1007/s10856-015-5403-9.
[44] B. Alberts, A. Johnson, J. Lewis, Ion Channels and the Electrical Properties of Membranes, Molecular Biology of the Cell, fourth ed., Garland Science, New York, 2002. https://www.ncbi.nlm.nih.gov/books/NBK26910/.
[45] M.F. Dilmore, D.E. Clark, L.L. Hench, Chemical durability of Na_2O-K_2O-CaO-SiO_2 glasses, J. Am. Ceram. Soc. 61 (1978) 439–443, https://doi.org/10.1111/j.1151-2916.1978.tb09355.x.
[46] V. Shirtliff, L.L. Hench, Bioactive materials for tissue engineering, regeneration and repair, J. Mater. Sci. 38 (2003) 4697–4707, https://doi.org/10.1023/A:1027414700111.
[47] S. Fagerlund, L. Hupa, M. Hupa, Dissolution patterns of biocompatible glasses in 2-amino-2-hydroxymethylpropane-1,3-diol (Tris) buffer, Acta Biomater. 9 (2013) 5400–5410, https://doi.org/10.1016/j.actbio.2012.08.051.
[48] A. Tilocca, Sodium migration pathways in multicomponent silicate glasses: car-Parrinello molecular dynamics simulations, J. Chem. Phys. 133 (2010), 014701, https://doi.org/10.1063/1.3456712.
[49] A. Tilocca, A.N. Cormack, Modeling the water-bioglass interface by ab initio molecular dynamics simulations, ACS Appl. Mater. Interfaces 1 (2009) 1324–1333, https://doi.org/10.1021/am900198t.
[50] H. Oonishi, L.L. Hench, J. Wilson, F. Sugihara, E. Tsuji, M. Matsuura, S. Kin, T. Yamamoto, S. Mizokawa, Quantitative comparison of bone growth behavior in granules of Bioglass, A-W glass-ceramic, and hydroxyapatite, J. Biomed. Mater. Res. 51 (2000) 37–46, https://doi.org/10.1002/(sici)1097-4636(200007)51:1<37::aid-jbm6>3.0.co;2-t.
[51] N.C. Lindfors, I. Koski, J.T. Heikkilä, K. Mattila, A.J. Aho, A prospective randomized 14-year follow-up study of bioactive glass and autogenous bone as bone graft substitutes in benign bone tumors, J. Biomed. Mater. Res., Part B 94 (2010) 157–164, https://doi.org/10.1002/jbm.b.31636.
[52] L.L. Hench, D.E. Clark, Physical chemistry of glass surfaces, J. Non-Cryst. Solids 28 (1978) 83–105.
[53] J. Hlaváč, D. Rohanová, A. Helebrant, The effect of TRIS-buffer on the leaching behaviour of bioactive glass-ceramics, Ceramics 38 (1994) 119–122.
[54] M. Siekkinen, O. Karlström, L. Hupa, Dissolution of bioactive glass S53P4 in a three-reactor cascade in continuous flow conditions, Open Ceramics (2023) 13 100327, https://doi.org/10.1016/j.oceram.2022.100327.
[55] J. Frantzén, Bioactive Glass in Lumbar Spondylodesis, a Pre-clinical and Clinical Study (PhD Thesis) Annales Universitatis Turkuensis, Ser. D 1029, Medica-Odontolgica, University of Turku, 2012.
[56] J.C. Elliott, Structure and Chemistry of the Apatites and Other Calcium Orthophosphates, first ed., Elsevier, Amsterdam, 1994.